Journal of Quantitative Spectroscopy & Radiative Transfer 236 (2019) 106599

Contents lists available at ScienceDirect

Journal of Quantitative Spectroscopy & Radiative Transfer

journal homepage: www.elsevier.com/locate/jqsrt

Super-efficient laser hyperthermia of malignant cells with core-shell nanoparticles based on alternative plasmonic materials

Artem S. Kostyukov[a,*], Alexander E. Ershov[a,b,c], Valeriy S. Gerasimov[a,b], Sergey A. Filimonov[a], Ilia L. Rasskazov[d], Sergey V. Karpov[a,c,e]

[a] Siberian Federal University, Krasnoyarsk, Russia
[b] Institute of Computational Modeling SB RAS, Krasnoyarsk, Russia
[c] Siberian State University of Science and Technology, Krasnoyarsk, Russia
[d] The Institute of Optics, University of Rochester, NY, USA
[e] Kirensky Institute of Physics, Federal Research Center KSC SB RAS, Krasnoyarsk, Russia

ARTICLE INFO

Article history:
Received 12 March 2019
Revised 31 July 2019
Accepted 1 August 2019
Available online 6 August 2019

Keywords:
Plasmonic photothermal therapy
Conducting oxides
Nanoparticle
Nanoshell

ABSTRACT

New type of highly absorbing core-shell AZO/Au (aluminum doped zinc oxide/gold) and GZO/Au (gallium doped zinc oxide/gold) nanoparticles have been proposed for hyperthermia of malignant cells purposes. Comparative studies of pulsed laser hyperthermia were performed for Au nanoshells with AZO core and traditional SiO_2 (quartz) core. We show that under the same conditions, the hyperthermia efficiency in the case of AZO increases by several orders of magnitude compared to SiO_2 due to low heat capacity of AZO. Similar results have been obtained for GZO core which has same heat capacity. Calculations for pico-, nano- and sub-microsecond pulses demonstrate that reduced pulse duration results in strong spatial localization of overheated areas around nanoparticles, which ensures the absence of negative effects to the normal tissue. Moreover, we propose new alternative way for the optimization of hyperthermia efficiency: instead of maximizing the absorption of nanoparticles, we enhance the thermal damage effect on the membrane of malignant cell. This strategy allows to find the parameters of nanoparticle and the incident radiation for the most effective therapy.

1. Introduction

Conjugates of plasmonic nanoparticles with biomacromolecules are one of the most important objects of interdisciplinary research with a great potential in biomedicine and biotechnology [1]. The increased interest in the study of these objects is explained by the fact that they represent a technological platform for the design of nanoscale biosensors of a new generation capable of detecting biomolecular interactions at the level of individual molecules. Biological complexes based on plasmonic nanoparticles are multifunctional, and can be simultaneously used both for diagnostics and for therapy, as well as for medical imaging and monitoring of the process of treatment of malignant tumors. In addition, these bioconjugates have low toxicity, which is especially important when using them as a part of complex therapy of oncological diseases and during their early diagnosis.

Plasmonic photothermal therapy (PPTT) was extensively developed during the last decade [2–10]. The main advantage of PPTT is thermally selective laser irradiation of malignant tumors which are labeled with plasmonic nanoparticles. Laser irradiation causes heating of the nanoparticles due to strong localization of electromagnetic field, local overheating and subsequent destruction of the cell membrane. Besides that, according to the opinion of authors [4,5], the destruction may occur due to formation of nano-sized bubbles of superheated steam around nanoparticles. Controllable death of malignant cells (apoptosis) takes place if the temperature of the tumor sites containing nanoparticles exceeds $\approx 43\,^{\circ}C$. The selectivity of exposure is based on the employing DNA aptamers [11–13] attached to Au surface of plasmonic nanoparticles, which allows them to bind to specific membrane proteins of the malignant cells. The targeting proprieties are formed by methods of its synthesis. Furthermore DNA aptamers are of particular interest due to their significantly smaller (≈ 3 nm) size, compared to antibodies. It allows to achieve the optimal heating regime of tumor cells with a low intensity of laser pulses.

In hyperthermia of tumors associated with local overheating of malignant cells conjugated with nanoparticles, it is especially important to ensure that the laser irradiation penetrates into tissue to the maximum depth and does not affect normal tissue [14,15].

* Corresponding author.
E-mail address: kostukov-a@yandex.ru (A.S. Kostyukov).

https://doi.org/10.1016/j.jqsrt.2019.106599
0022-4073/

Thus, the laser wavelength has to be within the transparency window of biological tissues and hemoglobin, and, obviously, overlap with the absorption band of nanoparticles. Therefore, the search of optimal plasmonic nanoparticle configurations capable to absorb effectively laser radiation in the transparency window, is of priority tasks of PPTT. Homogeneous spherical metal nanoparticles are poorly suited for these purposes. One of effective alternative way is to use multilayered nanoparticles with a dielectric core coated with a metallic shell (usually, Au) [16–18]. Employing Au core-shells ensures the biocompatibility of the multilayered particle and provides the unique ability of nanoparticle to adsorb aptamers. Multilayered spherical nanoparticles exhibit the maximum of plasmonic absorption in the near infrared spectral range, which coincides with the transparency band of hemoglobin and melanin. The coating of nanoparticle with other material (for example polyethylene glycol) can be used to control the spectral position of absorption maximum, to reduce the toxicity of particles and for binding with functional macromolecules [19].

Usually, in PPTT, only absorbing properties of nanoparticles are taken into account. A number of researches have addressed the problem of optimizing the absorption efficiency of core-shell spherical nanoparticles [20,21]. However, when using short laser pulses in a real environment, high-gradient, fast-relaxing thermal fields appear, and the temperature of the cell membrane near heating nanoparticle will depend on a number of factors. If the size of a particle with the maximum absorption is reduced, then this leads to a decrease in its heat capacity, which allows a particle to reach a higher temperature with the same amount of absorbed energy. However, with such a change in the geometric properties a particle loses the ability to maximize absorption and its absorption efficiency falls with size reduction. More detailed investigation of thermal response, temperature distribution, electron-phonon interaction inside plasmonic nanoparticles irradiated by short laser pulse were performed in [22–26]. Localization of the temperature fields around nanoparticle can be achieved only by using short laser pulses instead of continuous laser radiation [27]. Comprehensive calculations of heat transfer in human body for PPTT purposes have been performed in Refs. [28–32]. The role of melting of nanoparticle in high intensity laser fields was highlighted in Refs. [33–35].

The goal of this paper is to determine the structure of multilayered highly absorbing nanoparticles with Au nanoshells taking into account quantum finite-size effects, to perform comparative studies of the role of the core material consisting of both traditional dielectric materials (SiO_2) and new alternative plasmonic materials (AZO and GZO [36,37]) in the process of hyperthermia of the cell membrane. Mentioned in Ref. [36] new plasmonic material indium tin oxide (ITO) was not studied in detail in our paper due to its moderate toxicity [38]. Employing titanium nitride (TiN) [36] as the core or shell material does not allow to shift the absorption maximum to the spectral range of the hemoglobin transparency. Besides that we explore the effect of the pulse duration of laser radiation on the degree of spatial selectivity of the damage effect in the malignant cells. To achieve this goal, we have developed the theoretical model capable to describe the processes occurring in the “nanoparticle - cell membrane” system. The model includes the main parameters of the system, such as the geometric dimensions, electromagnetic and thermal properties of media, the parameters of external laser radiation, which allows to determine both the nanoparticle absorption efficiency and the efficiency of membrane damage.

2. Model

A system under consideration includes the following elements: a core-shell nanoparticle, aptamers adsorbed on the outer surface of the nanoparticle, a membrane of a malignant cell, and the environment, as shown in Fig. 1. We limit consideration to spherical nanoparticles of up to $\approx$80 nm diameter with either SiO_2 or AZO core and thin Au shell.

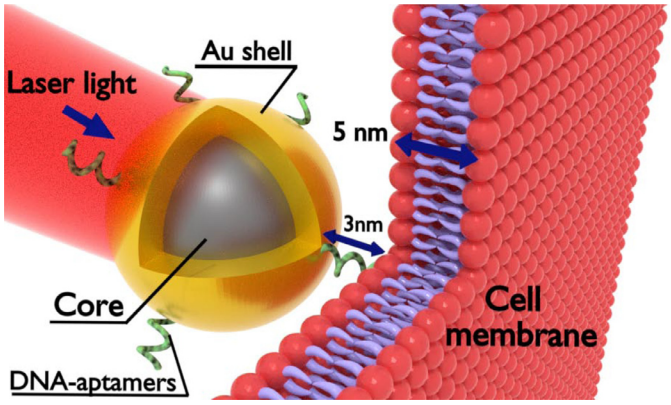

Fig. 1. Schematic representation of the considered system.

Since the size of a nanoparticle is much smaller than the characteristic size of cells, a membrane of the latter is considered as a flat layer with 5 nm thickness [39]. A particle is bound with the membrane of a malignant cell through a 3 nm sized DNA aptamer [11–13]. The size of the aptamers, which is determined by the number and sequence of nucleotides in their composition, is precisely controlled during their synthesis. In our case, the conformational state of the used aptamers in the form of a tangle determines its size equal to 3 nm [13]. Note, that in our paper we did not aim at studying the dependence of thermal parameters obtained with our model on the aptamer size.

The synthesized nanoparticles are located in an aqueous low-concentration electrolytic solution, in which an electric double layer is formed around the particles and prevents their coagulation [40]. The adsorption of aptamers on the surface of particles does not significantly affect the thickness of the electric double layer.

The environment is assumed to be homogeneous and non-absorbing. Laser radiation which is absorbed by the particle, causes local heating of both the particle and the environment. Under these conditions, the nearby area of the membrane is influenced by temperature fields near the particle, which leads to membrane destruction and subsequent cell death. It is assumed that the intercellular medium is homogeneous and optically transparent. Laser radiation, which is absorbed by particles, causes local heating of the particle and the local environment. Under these conditions, temperature fields around particles affect the nearby membrane area, which leads to membrane destruction and subsequent cell death.

The theoretical model includes the following processes:

- The absorption of the incident laser radiation by a particle, which is described by the absorption efficiency. The latter is determined by the structure of the particle, the properties of the materials composing it and depends on the wavelength of the incident radiation, which is necessary to calculate the temperature fields around the particle. The Mie theory for multilayered particles [41,42] was used to calculate absorption efficiency.
- The propagation of thermal energy in the vicinity of the particle. Calculations of the temperature of the particle include heating of its electron subsystem due to absorption of radiation and energy transfer to the crystal lattice. The thermal conductivity of nanoparticle’s materials is an order of magnitude higher than of the other components

of the model, therefore the nanoparticle temperature was considered to be the same throughout its volume at each iteration step. The cell membrane was considered as a homogeneous layer with constant thermal capacity and thermal conductivity. The transfer of thermal energy from the particle to the membrane and the heat distribution over the computational domain were calculated with the control volume method [43] on an irregular tetragonal grid. The NETGEN package was used to build up the grid. The solution of heat conduction equations was carried out according to a completely implicit scheme using the Pardiso package.

- Membrane heating results in the destruction of its lipids. This process is of a statistical nature, therefore, we consider a probability of destruction of the membrane, which leads to a cell death during thermal exposure, and describe it with the damage factor.

2.1. Absorption of electromagnetic radiation by core-shell nanoparticle

Scattering and absorption of light by a core-shell spherical nanoparticle are well defined from the solution of the appropriate electromagnetic problem [42]. For the sake of simplicity, we skip quite lengthy derivation and provide the final solution which is used in this work. For hyperthermia purposes, it is convenient to limit the discussion only to the absorption efficiency of a particle:

$$Q_a = \frac{2}{x_2^2}\sum_{n=1}^{\infty}(2n+1)\left[\mathrm{Re}\{a_n+b_n\} - |a_n|^2 - |b_n|^2\right] \quad (1)$$

where expansion coefficients a_n and b_n are defined as follows:

$$a_n = \frac{\psi_n(x_2)[\psi_n'(\tilde{m}_2x_2) - A_n\chi_n'(\tilde{m}_2x_2)] - \tilde{m}_2\psi_n'(x_2)[\psi_n(\tilde{m}_2x_2) - A_n\chi_n(\tilde{m}_2x_2)]}{\xi_n(x_2)[\psi_n'(\tilde{m}_2x_2) - A_n\chi_n'(\tilde{m}_2x_2)] - \tilde{m}_2\xi_n'(x_2)[\psi_n(\tilde{m}_2x_2) - A_n\chi_n(\tilde{m}_2x_2)]}$$

$$b_n = \frac{\tilde{m}_2\psi_n(x_2)[\psi_n'(\tilde{m}_2x_2) - B_n\chi_n'(\tilde{m}_2x_2)] - \psi_n'(x_2)[\psi_n(\tilde{m}_2x_2) - B_n\chi_n(\tilde{m}_2x_2)]}{\tilde{m}_2\xi_n(x_2)[\psi_n'(\tilde{m}_2x_2) - B_n\chi_n'(\tilde{m}_2x_2)] - \xi_n'(x_2)[\psi_n(\tilde{m}_2x_2) - B_n\chi_n(\tilde{m}_2x_2)]},$$

$$A_n = \frac{\tilde{m}_2\psi_n(\tilde{m}_2x_1)\psi_n'(\tilde{m}_1x_1) - \tilde{m}_1\psi_n'(\tilde{m}_2x_1)\psi_n(\tilde{m}_1x_1)}{\tilde{m}_2\chi_n(\tilde{m}_2x_1)\psi_n'(\tilde{m}_1x_1) - \tilde{m}_1\chi_n'(\tilde{m}_2x_1)\psi_n(\tilde{m}_1x_1)}$$

$$B_n = \frac{\tilde{m}_2\psi_n(\tilde{m}_1x_1)\psi_n'(\tilde{m}_2x_1) - \tilde{m}_1\psi_n(\tilde{m}_2x_1)\psi_n'(\tilde{m}_1x_1)}{\tilde{m}_2\chi_n'(\tilde{m}_2x_1)\psi_n(\tilde{m}_1x_1) - \tilde{m}_1\psi_n'(\tilde{m}_1x_1)\chi_n(\tilde{m}_2x_1)}$$

where $\xi_n(z) = \psi_n(z) - i\chi_n(z)$, $\psi_n(z)$ and $\chi_n(z)$ are Ricatti-Bessel functions, $\tilde{m}_{1,2} = m_{1,2}/m_g$ are normalized (to the surrounding medium with refractive index m_g) refractive indices of core and shell, respectively. Size parameters are: $x_{1,2} = 2\pi r_{1,2}/\lambda$, where $r_{1,2}$ is the outer radius of core and shell, correspondingly, and λ is the vacuum wavelength of the incident illumination.

The dielectric permittivity $\epsilon = m^2$ of non-magnetic Au shell with relatively thin thickness may significantly differ from the permittivity of bulk Au [44]. So-called finite-size effect (FSE) has to be taken into account, and the permittivity of Au is modified according to the following expression:

$$\epsilon_{Au} \longrightarrow \epsilon_{Au} + \frac{\omega_p^2}{\omega^2 + i\gamma_{\mathrm{bulk}}\omega} - \frac{\omega_p^2}{\omega^2 + i\gamma\omega}, \quad (2)$$

here $\omega = 2\pi c/\lambda$ is the incident frequency, ω_p is the plasma frequency, γ_{bulk} is the relaxation constant, and γ is [44]:

$$\gamma = \gamma_{\mathrm{bulk}} + A_L\frac{\upsilon_F}{L_e}, \quad (3)$$

here υ_F is Fermi velocity, L_e is average free path of conduction electrons A_L is dimensionless parameter, in most cases assumed to be close to unity [42]. For Au: $\gamma_{\mathrm{bulk}}/\omega_p = 0.00253$ and $\upsilon_F/c = 0.0046$ [45]. There are several ways to determine L_e [46,47], however, we use a simplified model: $L_e = r_2 - r_1$, which in our case gives an acceptable or even minor error [48] (r_2 and r_1 are outer and inner nanoshell radii).

2.2. Thermodynamics

Fig. 2 shows the computational domain with principal elements and the mesh refinement near the regions of strong heterogeneity: the boundaries “particle-water” and “water-membrane”.

The calculation of heat propagation includes two processes: heating the particle by incident laser radiation and the propagation of thermal energy into the medium surrounding the particle.

When calculating the particle heating by radiation in the model, the temperatures of the electron and ion (crystal lattice) subsystems of the particle material are taken into account separately. This is due to the short duration of the laser pulse, comparable with the characteristic energy transfer time between the electron and ion subsystems [35] and the value of the rate of heat transfer between the electron and ion subsystem [35]

$$W_{ex} = gV_p \cdot (T_e - T_i) \quad (4)$$

where W_{ex} is the power of heat transfer between electron and ion subsystem, V_p is the particle volume, g is the temperature-independent rate of energy exchange between the electron and ion subsystems above the Debye temperature [35], T_e and T_i are the temperatures of the electron and ion subsystem.

The distribution of the temperature of the electron and ion subsystems are assumed to be homogeneous throughout the volume of the particle. This approximation is acceptable due to the high thermal conductivity of the electron and ion subsystems compared to the thermal conductivity of the surrounding medium (water).

The applicability of this approach is justified by the fact that the final result of the calculations is the temperature value of the environment fragment in which the cell membrane is located. We should also note that the heating of a particle by radiation and heating of the environment by a particle have completely different kinetics. In the latter case, the heating rate is much slower. We aim our study first of all at the description of heating of the medium surrounding the particle, instead of a detailed description of the heating processes inside of the multilayered particle.

Thus, in this model, calculation of heating of the particle is carried out as follows:

- The temperature of the electron subsystem changes due to heating by external laser radiation (calculation is based on the effective absorption cross section of the multilayered particle and the intensity of radiation), as well as due to heat exchange with the ion subsystem. The heat capacity of the electron subsystem was assumed to be linearly dependent on the temperature: $C_e = 68 \cdot T_i[\frac{J}{m^3K}]$ [35].
- The temperature of the ion subsystem changes due to heat exchange with the electron subsystem and with the environment. The heat capacity of the ion subsystem of the particle was the sum of the heat capacities of the core and shell.

The calculation of the time dependence of the membrane temperature was performed using the non-stationary heat conduction equation:

$$\rho C\frac{\partial T}{\partial t} = \nabla(\alpha\nabla T). \quad (5)$$

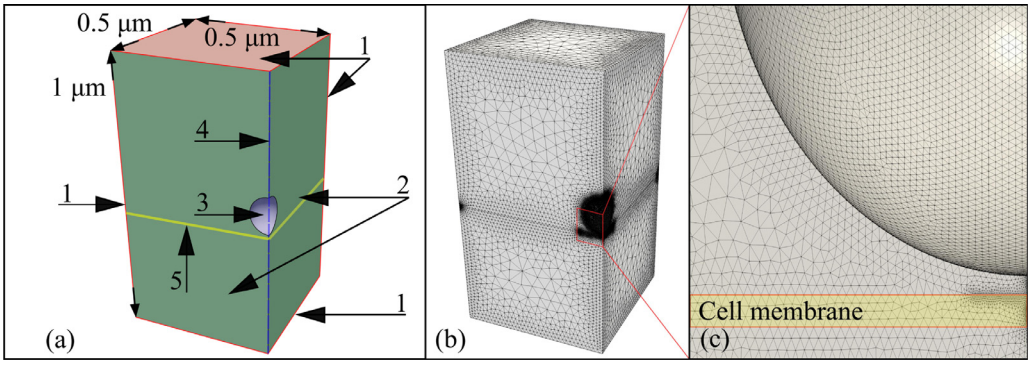

Fig. 2. (a) The schematic representation of the computational domain with 124 nm particle inside. There are three different kinds of boundaries: 1 – the outer boundary, 2 – the symmetry boundary, 3 – the particle-water interface. 4 – the symmetry axis, and 5 – the membrane position; (b) Fragmentation of the domain to small computational volumes with variable size; (c) Enhanced details of fragmentation near the particle and membrane.

Table 1
Properties of materials used in the model.

Material	ρ, kg/m^3	C, J/(kg · K)	α, W/(m · K)	Ref.
Water	1000	4183	0.6	
Membrane	920	1550	0.43	[49]
AZO, GZO	5610	495	-	[50,51]
Au	19,320	130	-	[51]
SiO_2	2650	750	-	[51]

Here ρ is a volume density, C is a specific heat, and α is a heat conductivity. Values of ρ, C and α for different materials used in the model are given in the Table 1.

The doping level of AZO with aluminum is insignificant (2 wt% [37]). This level considerably affects the optical properties of the material, but the effect on the heat capacity is negligible [52].

The size of the area under consideration and the characteristic times of the processes allow us to neglect the influence of convection. Of note, Eq. (5) can be used if $T/|\nabla T|$ is larger than the intermolecular distance [53] (0.2 nm for water), which is valid for the considered system.

The method of control volumes [43] was used for solving and discretizing the Eq. (5) within the computational domain. The solution was carried out using a completely implicit first order accuracy scheme. The three types of boundary conditions were used:

- The temperature of the outer boundary (1) In Fig. 2a of the computational domain was assumed to be equal to the temperature of the human body ($T_0 = 310$ K $= 36.85$ °C). The boundaries of the computational domain were determined by the condition of negligible heating of the water in the domain volume by a particle. Considering that, the size of the domain was taken to be 1 μm. This is a characteristic cell size and, accordingly, the distance between the centers of the two nearest cells (intercellular distance).
- To reduce the calculation time, the domain was split into a quarter of the original size. A symmetry condition was set at the boundaries (for boundary (2) in Fig. 2b: the heat flux was set to zero).
- The temperature of water-particle boundary — (3) in Fig. 2a is equal to the temperature of the particle at every moment of time.

To perform calculations for particles of different diameters, it is necessary to rebuild the mesh. We used NETGEN library for that purpose [54], which allows to generate tetrahedral meshes for Constructive Solid Geometry. The solution of the system of linear equations was performed using the Pardiso package [55].

2.3. Damage factor

The process of thermal destruction of the cell membrane is associated with the dissolution of its lipids in the surrounding aqueous electrolytic medium and the conformational transitions of the membrane proteins [56]. This process can be described by a simple first order kinetics equation of chemical reaction. The following equations, which are analogous of the Arrhenius equation, can be used to describe the impact resulting in the destruction of the cell membrane [27,56]:

$$\begin{aligned} \frac{dN(t)}{dt} &= -\frac{d\Omega(t)}{dt}N(t) \\ N(t=0) &= N_0 \\ \frac{d\Omega(t)}{dt} &= A_r e^{-E/RT(t)}. \end{aligned} \tag{6}$$

Here N is the number of living cells, N_0 is the initial number of cells, A_r characterizes the frequency of collisions between interacting molecules at $T \to \infty$, R is the universal gas constant, $T(t)$ is the time dependence of the absolute temperature of the cell membrane, E [J/mol] is the energy required for the destruction of the cell membrane per 1 mol of molecules included in its composition [56]. Damage factor Ω is determined by integrating the Eq. (6) over the heat exposure time:

$$\Omega(t) = \int_0^t A_r e^{-E/RT(t)} dt \tag{7}$$

which characterizes the degree of the membrane damage. The following values were used: $A_r = 2.9 \times 10^{37}$ sec^{-1} and $E = 244$ kJ/mol, which correspond to muscle cells [56].

Thus, the fraction of damaged cells is determined by the equation:

$$k(t) = 1 - \frac{N(t)}{N_0} = 1 - e^{-\Omega(t)}. \tag{8}$$

A membrane destruction is also considered as a condition for a cell death.

3. Results

3.1. Single particle absorption spectra

The efficiency of the PPTT strongly depends on various factors, however, the most important one is the wavelength of the incident illumination. In most of the cases, malignant cells are located deep inside the tissue (except for skin and oral cancers), thus, the incident laser irradiation can be strongly absorbed by hemoglobin before reaching the nanoparticle and malignant cell. In this case,

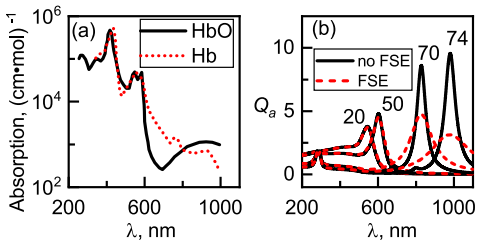

Fig. 3. (a) Optical absorption of deoxyhemoglobin (Hb) and oxyhemoglobin (HbO); (b) Absorption spectra of AZO/Au particles with $d_{sh} = 80$ nm for different values of d_c which is shown (in nanometers) above each peak of the corresponding curve. Calculations are performed with and without consideration of quantum finite-size effects, Eq. (2).

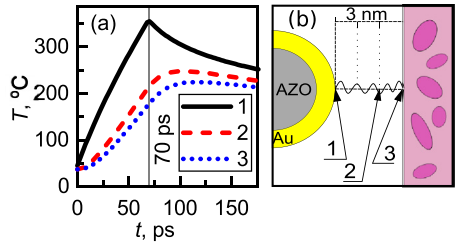

Fig. 4. (a) Time-resolved temperature distribution near AZO/Au nanoparticle with $d_c = 54.5$ nm and $d_{sh} = 68.5$ nm: 1 – at nanoparticle's surface, 2 – at 2 nm distance from nanoparticle's surface, 3 – at membrane's surface. (b) Schematic representation of the system.

not only the efficient PPTT becomes impossible, but normal cells can be damaged as well, due to the overheating. To mitigate this issue, it is convenient to operate in the near-infrared wavelength range, which corresponds to so-called biological transparency window where the absorption of hemoglobin is negligible, as shown in Fig. 3(a) for $\lambda > 600$ nm. Therefore, in this work, we assume that nanoparticles are illuminated with either tunable Alexandrite laser ($700\,\text{nm} \le \lambda \le 800\,\text{nm}$) or a neodymium laser ($\lambda = 1064$ nm).

The choice of the appropriate material and shape of plasmonic nanoparticle for efficient PPTT becomes quite challenging task. However impressive number of various strategies have been discussed in a recent decade with particular interest to Au nanorods and spherical SiO_2/Au core-shell nanoparticles. These two configurations of nanoparticles attract significant attention since both of them exhibit strong surface plasmon resonances in near-IR.

In this work, we limit the discussion to the core-shell spherical nanoparticles, however, along with SiO_2/Au we consider AZO/Au configuration which has similar optical properties [21]. We describe the particle's geometry with two independent parameters: the total particle diameter d_{sh} and the diameter of the core d_c.

Fig. 3(b) shows the absorption efficiency of AZO/Au nanoparticle with fixed $d_{sh} = 80$ nm and varying d_c. It can be seen that core-shell nanosphere has tunable optical properties, and the absorption peak of the nanoparticle can be easily shifted from visible to near-IR range upon increase of the core size. However, it is important to draw attention to the emergence of FSE which may affect the Q_a. For thick Au shell (up to 15 nm) FSE does not play a significant role, however, with its further decrease, FSE becomes substantial and suppresses resonance, keeping its spectral position the same.

3.2. Calculation of temperature fields

Although the absorption spectrum of core-shell nanoparticle provides quite useful information regarding the optimal regime of its illumination, the local heating and the radiative heat transfer from nanoparticle to the cell requires a deeper investigation in order to get insight into the thermal processes.

Fig. 4(a) shows time-dependent temperature for AZO/Au nanoparticle illuminated with 70 ps laser pulse at $\lambda = 701$ nm. It can be seen that the nanoparticle reaches its maximum temperature at $t = 70$ ps (which corresponds to the pulse end) and releases energy to the surrounding medium after the pulse end. At the same time, the membrane continues to heat up for 46 ps after the pulse end ($t = 116$ ps). The temperature of the nanoparticle quickly falls down, and after ≈ 100 ps, it reaches the temperature of the membrane. Thus, one may expect the existence of pronounced temperature gradients between the nanoparticle and the membrane.

The heat capacity of nanoparticle corresponds to its volume. Smaller particles have lesser heat capacity that allows them to reach higher temperatures at the short time, and the opposite trend takes place for the larger particles. Fig. 5 demonstrates this effect. We show the temperature distribution between the nanoparticle surface and the membrane at different moments of time for two particles with different sizes and same core/shell ratio. Despite the fact that a large particle has a larger absorption efficiency: $Q_a^{(1)} = 5.655$ vs $Q_a^{(2)} = 5.563$ for large and small particle, respectively, a smaller particle heats up faster to higher temperatures and cools faster. It can be seen from Fig. 5(c) that at $t = 750$ ps, the temperature of a system for smaller particle falls to lower values compared to the larger particle. However, the damage factor, which is an integral value according to Eq. (7), for a smaller particle turns out to be larger: $\Omega^{(1)} = 19.7$ vs $\Omega^{(2)} = 47.6$. Thus, it can be seen that the highest absorption efficiency does not necessarily imply the best damage factor, and comprehensive thermodynamic study is required for the search of optimal nanoparticle configuration for the efficient PPTT.

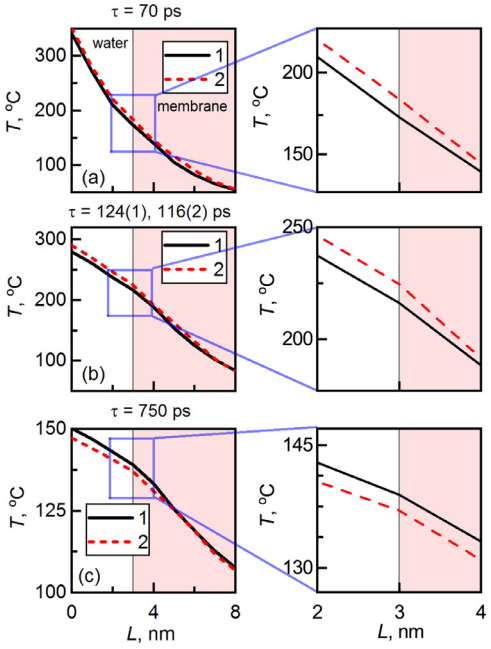

Fig. 5. The temperature distribution in the nearest direction to the membrane at different moments: (a) at the pulse end, $\tau = 70$ ps, (b) at the moment of reaching the maximum temperature of membrane, $\tau^{(1)} = 124$ ps and $\tau^{(2)} = 116$ ps for particles 1 and 2, respectively, (c) at $\tau = 750$ ps. Particle 1: $d_c = 58.5$ nm, $d_{sh} = 74.0$ nm, $\lambda = 700$ nm, particle 2: $d_c = 54.5$ nm, $d_{sh} = 68.5$ nm, $\lambda = 701$ nm. L is the distance from the surface of a particle. $L = 0$ nm corresponds to the particle surface, $L = 3$ nm is the outer surface of the membrane, $L = 8$ nm is the internal surface of the membrane.

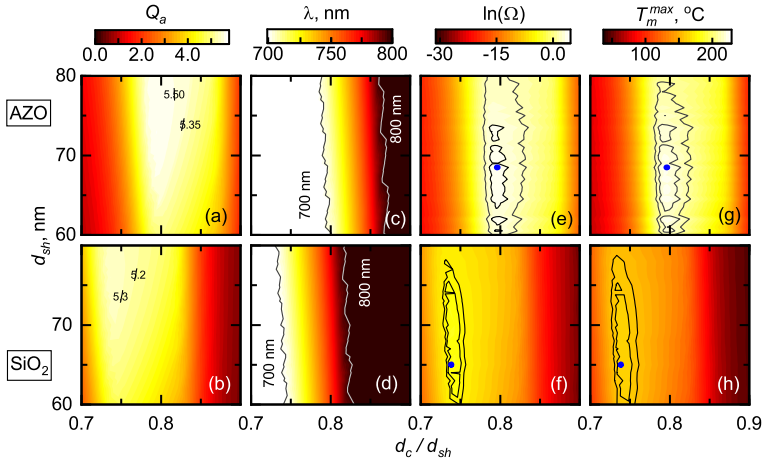

Fig. 6. (a),(b) Absorption efficiency Q_a, (c),(d) corresponding wavelength λ, (e),(f) damage factor ln(Ω), and (g),(h) maximum temperature of the membrane $T_m^{\max}$ for AZO/Au (top) and SiO_2/Au (bottom) core-shell nanoparticles in 700 – 800 nm spectral range and 70 ps pulse duration.

Table 2
The parameters of AZO/Au and SiO_2/Au particles with the maximum absorption and the maximum damage factor.

	Max absorption (A)		Max damage (D)	
Parameter	AZO/Au	SiO_2/Au	AZO/Au	SiO_2/Au
d_c, nm	58.5	56.0	54.5	48.0
d_{sh}, nm	74.0	76.0	68.5	65.0
λ, nm	700	701	701	700
Q_a	5.655	5.39	5.563	5.09
Ω	19.7	0.011	47.6	0.022
T_p^{max}, °C	344.8	228.7	355.3	242.1
T_m^{max}, °C	216.2	157.4	224.6	163.3

3.3. Effect of the structure of a multilayered particle on its heating and damage to the cell membrane

It becomes obvious from Figs. 3–5 that the search for optimal configuration of the particles for efficient PPTT is a non-trivial task. In this section, we provide comprehensive calculations to fulfill this need. We analyze optical and thermal properties of core-shell particles with AZO or SiO_2 core and Au shell. The diameters of the nanoparticle d_{sh} and the diameter of the core d_c were changed from 40 to 80 nm with a step of 0.5 nm. The maximum of the absorption efficiency for such nanoparticles lies within the 700–800 nm wavelength range, which corresponds to the tunability range of the Alexandrite laser.

We start with the absorption efficiency shown in Fig. 6(a) and (b). The calculations were performed at the wavelengths which correspond to the peak (or maximum value) of Q_a for each particular geometrical configuration within 700 – 800 nm spectral range, as shown in Fig. 6(c) and (d). It can be seen that an optimal configuration with the highest Q_a exists for both AZO and SiO_2 cores. In Fig. 6(a) and (b) we mark this optimal configuration with blue dots. The geometrical parameters for both of these particles are given in Table 2. Hereinafter we will refer to these particles with the superscript A: the absorption efficiency for optimally absorbing AZO/Au particle is $Q_a^A = 5.655$ and for SiO_2 is $Q_a^A = 5.39$.

Fig. 6(e) and (f) show the corresponding damage factor Ω caused by $\tau = 70$ ps laser pulse. Since Ω is the integral of an exponential function, according to Eq. (7), it is convenient to show it in a logarithmic scale, i.e. ln(Ω). As in the case for the Q_a, one could observe the existence of the configuration with the maximum Ω, which is again marked with the blue dots in Fig. 6(e) and (f). It can be seen that generally, the particle with the highest Ω is smaller than the particle with the highest Q_a, but almost with the same d_c/d_{sh} ratio. Hereinafter we will refer to these particles with the superscript D: the damage factor for optimally heated AZO/Au particle is $\Omega^D = 47.6$ and for SiO_2 is $\Omega^D = 0.022$. Of note, corresponding values of damage factor for optimally absorbing particles are: $\Omega^A = 19.7$ and $\Omega^A = 0.011$.

It is also important to calculate the maximum temperature T_m^{max} of the membrane during exposure, as shown in Fig. 6(g) and (h). It can be seen that $\Delta T^A = 179.2°C$ and $\Delta T^D = 187.6°C$ for AZO/Au nanoparticles. This means that the particle D heats the membrane to 4.7% higher temperature than the particle A. The same calculation for SiO_2/Au particle gives 4.9% difference between ΔT^A and ΔT^D.

At high temperatures, the water can vaporize with the subsequent formation of vapor nanobubbles around particles, which can also damage the cell membrane [4]. However, it was shown in [57] that the nanobubbles are created only with spinodal crossing, if a finite volume of liquid around a particle (~10 nm from surface) is heated above critical spinodal temperature (~277 °C). In our case, the temperature of aqueous medium at distances larger than 3 nm from a particle does not exceed 224 °C, which is not enough for a bubble formation.

All of malignant cells will be destructed under the influence of radiation with optimal intensity, which yields in $\Omega = 47.6$ and $\Omega = 19.7$. However, lower radiation intensity will cause rapid decrease of the fraction of destructed cells. Radiation intensity determines the temperatures of nanoparticles and the cell membrane, according Eq. (7). The higher the damage factor the higher the fraction of damaged malignant cells at lower intensity which is demonstrated in Fig. 7. The particle D requires lower fluence of irradiating light than the particle A for reaching the same level of cell death (for example 0.88 mJ/cm^2 and 0.92 mJ/cm^2 comparatively for 95% death cell ratio).

More significant influence on the ratio k in Eq. (8) will be observed with changing the material of a core. As can be seen the optical absorption of particles with a core of AZO and SiO_2 and the same Au shell does not differ much from each other, however, the efficiency of damage to the cell membrane of SiO_2/Au particles is significantly less than that of AZO/Au particles due to the high heat capacity of SiO_2. According to Eq. (8), the fraction of damaged malignant cells at the values of damage factor $\Omega = 47.6$ and $\Omega = 0.02$ equal to $k = 1$ and $k = 0.02$, for AZO/Au and SiO_2/Au nanoparticles, respectively. Thus, not only the ability of the

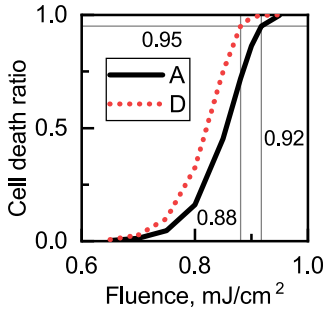

Fig. 7. Cell death ratio $k = 1 - N/N_0$ (Eq. (8)) as a function of radiation fluence during the thermalization period of the system and its return to the initial state. Radiation fluence J=1.0 mJ/cm^2 corresponds to the intensity I = 14.3 MW/cm^2 for τ=70 ps laser pulse.

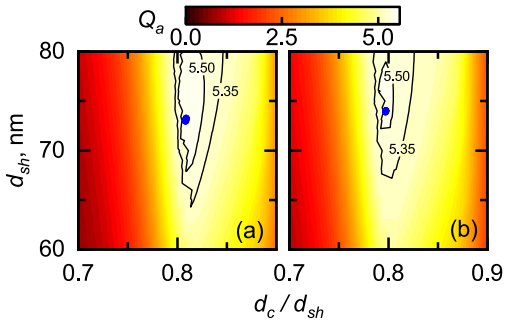

Fig. 8. Absorption efficiency Q_a for (a) GZO/Au and (b) ITO/Au core-shell nanoparticles.

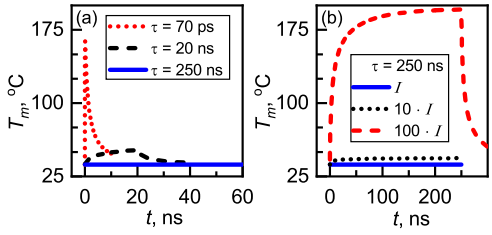

Fig. 9. (a) Time-dependence membrane temperature during irradiation of laser pulses of different duration (τ) at the intensity values $I = 1.0$ [mJ/cm^2] $\cdot\ \tau^{-1}$[s^{-1}], SiO_2/Au particle sizes are $d_c = 48$ nm, $d_{sh} = 65$ nm. (b) The same for a submicrosecond laser pulse with an increasing the radiation intensity per pulse, where $I = 1.0$ [mJ/cm^2] $\cdot\ \tau^{-1}$[s^{-1}].

material of a particle to absorb incident laser radiation of a selected wavelength, but also the thermophysical properties of the core material affects the efficiency of the system under study.

Similar results for absorption efficiency have been obtained for GZO/Au and ITO/Au nanoparticles. Comparison of the spectra for these core materials are shown in Fig. 8 which are similar to AZO/Au nanoparticles with the same sizes shown in Fig. 6(a). Similar heat capacities for AZO and GZO are reported in Refs. [50,51], which along with high particle absorption efficiency contribute to large values of the damage factor.

Another important tendency was found when the duration of a laser pulse decreases from submicrosecond to picosecond with the same fluence: significantly higher temperature gradients are observed near the membrane, as shown in Fig. 9(a). This ensures a high localization and selectivity of the thermal effect on malignant cells with attached nanoparticles heated by laser radiation.

Fig. 9(b) shows that the same temperature of membrane can be reached for picosecond and submicrosecond pulsed radiation only if the radiation fluence of submicrosecond pulses will be hundred

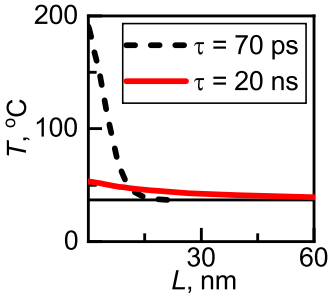

Fig. 10. Temperature distribution near SiO_2/Au particle when it is exposed to the Alexandrite pulsed laser radiation of different pulse duration at the moment when the temperature of membrane is maximum. For the 70 ps pulse, the membrane reaches maximum temperature at t=134 ps.

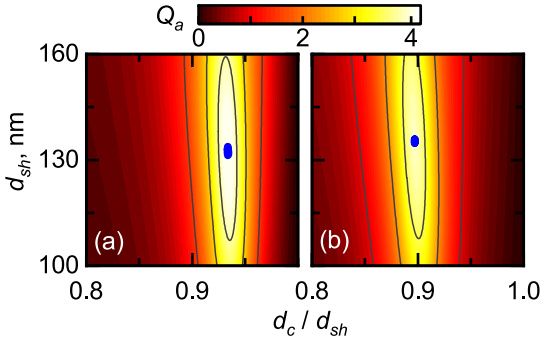

Fig. 11. The absorption spectra of (a) AZO/Au and (b) SiO_2/Au nanoparticles at λ = 1064 nm.

times higher. Comparative localization areas for 70 ps an 20 ns pulse are shown at Fig. 10.

The temperature distribution after the 20 ns pulse have significantly lower magnitudes near a particle and membrane but the temperature slowly reduces with distance. The dangerous temperature values for normal tissue can be observed at the distance over 30 nm. Short pulse with $\tau = 70$ ps provides the localized temperature distribution sufficient for destruction the malignant cells within the 15 nm distance; the heating beyond this area is negligible.

3.4. Interaction of core-shell particles with Nd:YAG laser radiation

One of the widely used types of lasers applied in medicine are neodymium lasers with a radiation wavelength 1064 nm. In this paper, we investigate the possibility of employing nanoparticles with a core-shell structure and positions of a resonance band coinciding with the wavelength range of a neodymium laser for the problems of laser hyperthermia.

Fig. 11 demonstrates the absorption efficiency of the AZO/Au and SiO_2/Au particles at $\lambda = 1064$ nm corresponding to the radiation of the neodymium laser.

First of all, calculations show that the size of such particles is doubled in comparison with particles for the range of 700 – 800 nm of an Alexandrite laser. The volume of the particle significantly grows, that negatively affects heat capacity of the particle and the temperature near the membrane that is demonstrated by Fig. 12. Calculations of the temperature fields and the damage factor were carried out for particles AZO/Au and $\lambda = 1064$ nm. The results are presented in Fig. 12(a).

Fig. 12(b) shows the time dependence of the membrane temperature when ideally absorbing particles are subjected to the radiation of Alexandrite ($\lambda = 700$ nm) and neodymium

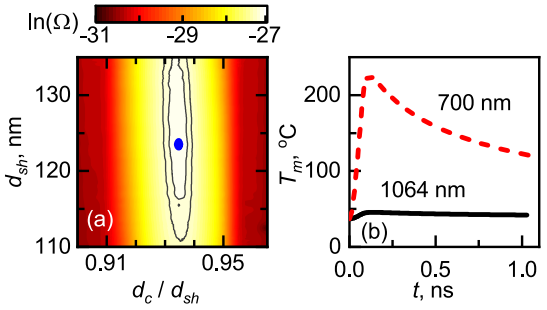

Fig. 12. (a) The damage factor of AZO/Au particles at wavelength $\lambda = 1064$ nm; (b) Time dependence of the membrane temperature T_m when a particle is exposed to pulsed radiation of Alexandrite ($\lambda = 700$ nm) and neodymium ($\lambda = 1064$ nm) lasers with pulse duration 70 ps with same radiation intensity.

($\lambda = 1064$ nm) lasers. Figures demonstrate that when ideally absorbing particles with maximum absorption in the range of $\lambda = 700 - 800$ nm are irradiated by a laser pulse, a much stronger heating of the membrane of the malignant cell is observed compared to particles with a resonant band near 1064 nm with the same energy and pulse duration.

4. Conclusion

Application of bioconjugates of ideally absorbing multilayered particles based on alternative plasmonic materials opens up new possibilities in increace of the efficiency of photothermal therapy, despite the technological difficulties associated with synthesis of such particles. Such particles make it possible to shift the absorption maximum into the hemoglobin transparency spectral band, significantly reduce the intensity threshold of pulsed laser radiation to avoid damage effects on normal cells, and to localize the destructive temperature field near the particle.The considered nanomaterials can be used in the form of electrostatically stabilized hydrosols resistant to coagulation of particles.

A model has been developed that allows one to describe the interaction of a multilayered plasmonic nanoparticle with optical radiation and calculate temperature effect to the membrane of malignant cell. The system of cell membrane in aqueous medium and bioconjugates based on the DNA-aptamer modified core-shell nanoparticles with a golden shell have been studied. The absorption spectra and the values of the damage factor were obtained for particles by various sizes of the core and shell thickness.

It was shown that the particles with maximum absorption (particles A) and with maximum damage factor (particles D) may have slightly different sizes (exact values of the particle parameters are in Table 2).

Aluminum doped zinc oxide (AZO) is a promising plasmonic material with low internal losses for the near IR range was used and investigated as a core material. Comparative studies of pulsed laser hyperthermia of malignant cells were performed using nanoparticles with a core from both AZO and traditional materials by example of SiO_2. It has been shown that under the same conditions, the efficiency of damage of the cell membrane in hyperthermia with nanoparticles with an the AZO core increases by several orders of magnitude compared to the quartz core due to low heat capacity of AZO. Similar results have been obtained for GZO as the core materials with low heat capacity.

The importance of using in hyperthermia the picosecond laser pulses has been shown. Picosecond pulses allow one to concentrate the heat energy in the small volume around the particle. Localization of the heating area increases the thermal effect to the malignant cell membrane and decreases the destructive effect to normal cells adjacent to the particle.

The study of the possibility of employing nanoparticles with a core-shell structure and a resonant band coinciding with the radiation wavelength range of a neodymium laser, 1064 nm, for laser hyperthermia shows that the size of such particles doubles compared to the particles for the 700–800 nm range of Alexandrite laser. At the same time, the required thickness of Au shell is reduced to 10 nm or less, which is accompanied by the manifestation of a quantum size effect. This effect significantly worsens the resonant properties of particles and the efficiency of their interaction with radiation. In addition, a twofold increase in the size results in an increase in the heat capacity of the particles. It will not allow the particle to heat up to the threshold temperature of the membrane destruction. This will require a significant increase in the laser radiation intensity accompanied in such conditions by damage to the normal cells. Thus, we note that the effective localized hyperthermia of malignant cells by pulsed radiation of a neodymium laser with the wavelength of 1064 nm faces serious difficulties. On the other hand application of this radiation has an advantage in the case when there is a need for penetration of radiation into the deeper layers of tissue.

All of mentioned above factors such as the size and the structure of particles, the heat capacity of particles and their material, the laser pulse duration and the radiation wavelength, the kinetics of high gradient temperature fields near a particle, the heating of the particle and the environment have a great effect and determine the maximum achievable value of the damage factor. They must be taken into account in optimization of PPTT problems.

We also draw an attention to the fact that the high heat capacity of traditional dielectric materials of the core in multilayered nanoparticles becomes an obstacle to the further optimization of photothermal methods for treating oncological diseases.

Acknowledgments

The reported study was funded by the RF Ministry of Science and Higher Education, the State contract with Siberian Federal University for scientific research in 2017–2019 (Grant No. 3.8896.2017); Russian Foundation for Basic Research, Government of Krasnoyarsk Territory, Krasnoyarsk Regional Fund of Science (Grant No.18-42-243023); A.E. thanks the grant of the President of Russian Federation (agreement 075-15-2019-676).

References

[1] Khlebtsov NG. Optics and biophotonics of nanoparticles with a plasmon resonance. Quantum Electron 2008;38(6):504–29.
[2] Terentyuk GS, Maslyakova GN, Suleymanova LV, Khlebtsov NG, Khlebtsov BN, Akchurin GG, et al. Laser-induced tissue hyperthermia mediated by gold nanoparticles: toward cancer phototherapy. J Biomed Opt 2009;14(2):021016.
[3] Huang X, Jain PK, El-Sayed IH, El-Sayed MA. Plasmonic photothermal therapy (PPTT) using gold nanoparticles. Lasers Med Sci 2008;23(3):217–28.
[4] Lapotko D. Plasmonic nanoparticle-generated photothermal bubbles and their biomedical applications. Nanomedicine 2009;4(7):813–45.
[5] Lukianova-Hleb E, Hu Y, Latterini L, Tarpani L, Lee S, Drezek RA, et al. Plasmonic nanobubbles as transient vapor nanobubbles generated around plasmonic nanoparticles. ACS Nano 2010;4(4):2109–23.
[6] Qin Z, Bischof JC. Thermophysical and biological responses of gold nanoparticle laser heating. Chem Soc Rev 2012;41(3):1191–217.
[7] Jaque D, Martínez Maestro L, del Rosal B, Haro-Gonzalez P, Benayas A, Plaza JL, et al. Nanoparticles for photothermal therapies. Nanoscale 2014;6(16):9494–530.
[8] Abadeer NS, Murphy CJ. Recent progress in cancer thermal therapy using gold nanoparticles. J Phys Chem C 2016;120(9):4691–716.
[9] Khanadeev VA, Khlebtsov BN, Khlebtsov NG. Optical properties of gold nanoshells on monodisperse silica cores: experiment and simulations. J Quant Spectrosc RadiatTransf 2017;187:1–9.
[10] Chen Q, Qi H, Ruan L, Ren Y. Experimental comparison of photothermal conversion efficiency of gold nanotriangle and nanorod in laser induced thermal therapy. Nanomaterials 2017;7(12).
[11] Zhang J, Liu B, Liu H, Zhang X, Tan W. Aptamer-conjugated gold nanoparticles for bioanalysis. Nanomedicine 2013;8(6):983–93.
[12] Reinemann C, Strehlitz B. Aptamer-modified nanoparticles and their use in cancer diagnostics and treatment. Swiss Med Weekly 2014.

[13] Zamay GS, Kolovskaya OS, Zamay TN, Glazyrin YE, Krat AV, Zubkova O, et al. Aptamers selected to postoperative lung adenocarcinoma detect circulating tumor cells in human blood. Mol Ther 2015;23(9):1486–96.
[14] Xin Y, Yin M, Zhao L, Meng F, Luo L. Recent progress on nanoparticle-based drug delivery systems for cancer therapy. Cancer Biol Med 2017;14(3):228.
[15] Ren Y, Qi H, Chen Q, Ruan L. Thermal dosage investigation for optimal temperature distribution in gold nanoparticle enhanced photothermal therapy. Int J Heat Mass Transf 2017;106:212–21.
[16] Hirsch LR, Stafford RJ, Bankson JA, Sershen SR, Rivera B, Price RE, et al. Nanoshell-mediated near-infrared thermal therapy of tumors under magnetic resonance guidance. Proc Natl Acad Sci 2003;100(23):13549–54.
[17] Hirsch LR, Gobin AM, Lowery AR, Tam F, Drezek RA, Halas NJ, et al. Metal nanoshells. Annal Biomed Eng 2006;34(1):15–22.
[18] Ghosh Chaudhuri R, Paria S. Core/shell nanoparticles: classes, properties, synthesis mechanisms, characterization, and applications. Chem Rev 2012;112(4):2373–433.
[19] Chen Q, Ren Y, Qi H, Ruan L. Influence of peg coating on optical and thermal response of gold nanoshperes and nanorods. J Quant Spectrosc Radiat Transf 2018;212:1–9.
[20] Tuersun P, Han X. Optical absorption analysis and optimization of gold nanoshells. Appl Opt 2013;52(6):1325.
[21] Zakomirnyi VI, Rasskazov IL, Karpov SV, Polyutov SP. New ideally absorbing Au plasmonic nanostructures for biomedical applications. J Quant Spectrosc RadiatTransf 2017;187:54–61.
[22] Lahiri A, Mondal PK. Evaluation of temperature history of a spherical nanosystem irradiated with various short-pulse laser sources. Phys Rev E 2018;97(4):043302.
[23] Xu M, Yang J-Y, Zhang S, Liu L. Role of electron-phonon coupling in finite-temperature dielectric functions of Au, Ag, and Cu. Phys Rev B 2017;96(11):115154.
[24] Alabastri A, Toma A, Malerba M, De Angelis F, Proietti Zaccaria R. High temperature nanoplasmonics: the key role of nonlinear effects. ACS Photonics 2015;2(1):115–20.
[25] Avetisyan YA, Yakunin AN, Tuchin VV. Thermal energy transfer by plasmon-resonant composite nanoparticles at pulse laser irradiation. Appl Opt 2012;51(10):C88.
[26] Avetisyan YA, Yakunin AN, Tuchin VV. Novel thermal effect at nanoshell heating by pulsed laser irradiation: hoop-shaped hot zone formation. J Biophoton 2012;5(10):734–44.
[27] Gerasimov VS, Ershov AE, Karpov SV, Polyutov SP, Semina PN. Optimization of photothermal methods for laser hyperthermia of malignant cells using bioconjugates of gold nanoparticles. Colloid J 2016;78(4):435–42.
[28] Dombrovsky LA, Timchenko V, Jackson M, Yeoh GH. A combined transient thermal model for laser hyperthermia of tumors with embedded gold nanoshells. Int J Heat Mass Transf 2011;54(25–26):5459–69.
[29] Dombrovsky LA, Timchenko V, Jackson M. Indirect heating strategy for laser induced hyperthermia: an advanced thermal model. Int J Heat Mass Transf 2012;55(17–18):4688–700.
[30] Timchenko V, Dombrovsky L. Laser induced hyperthermia of superficial tumors:a transient thermal model for indirect heating strategy. Comput Thermal Sci 2012;4:457–75.
[31] Yu D-M, Liu Y-N, Tian F-L, Pan X-M, Sheng X-Q. Accurate thermoplasmonic simulation of metallic nanoparticles. J Quant Spectrosc RadiatTransf 2017;187:150–60.
[32] Dombrovsky LA, Timchenko V, Pathak C, Piazena H, Mller W, Jackson M. Radiative heating of superficial human tissues with the use of water-filtered infrared-a radiation: a computational modeling. Int J Heat Mass Transf 2015;85:311–20.
[33] Gerasimov VS, Ershov AE, Gavrilyuk AP, Karpov SV, Ågren H, Polyutov SP. Suppression of surface plasmon resonance in au nanoparticles upon transition to the liquid state. Opt Express 2016;24(23):26851.
[34] Gerasimov VS, Ershov AE, Karpov SV, Gavrilyuk AP, Zakomirnyi VI, Rasskazov IL, et al. Thermal effects in systems of colloidal plasmonic nanoparticles in high-intensity pulsed laser fields [Invited]. Opt Mater Express 2017;7(2):555.
[35] Ershov AE, Gerasimov VS, Gavrilyuk AP, Karpov SV. Surface plasmon resonances in liquid metal nanoparticles. Appl Phys B 2017;123(6):182.
[36] Naik GV, Kim J, Boltasseva A. Oxides and nitrides as alternative plasmonic materials in the optical range [Invited]. Opt Mater Express 2011;1(6):1090.
[37] Naik GV, Shalaev VM, Boltasseva A. Alternative plasmonic materials: beyond gold and silver. Adv Mater 2013;25(24):3264–94.
[38] Homma S, Miyamoto A, Sakamoto S, Kishi K, Motoi N, Yoshimura K. Pulmonary fibrosis in an individual occupationally exposed to inhaled indium-tin oxide. Eur Respirat J 2005;25(1):200–4.
[39] Kuchel PW, Ralston GB, Bersten AM, Easterbrook-Smith SB, Jones AR, Montague MD, et al. Schaum's outline of theory and problems of biochemistry. 2nd. New York, United States: McGraw-Hill; 1998. ISBN 9780585306087.
[40] Sonntag H, Strenge K. Coagulation and stability of disperse systems. Israel Progr Sci Translat; 1972. ISBN 9780706511062.
[41] Wu ZS, Wang YP. Electromagnetic scattering for multilayered sphere: recursive algorithms. Radio Sci 1991;26(6):1393–401.
[42] Bohren CF, Huffman DR. Absorption and Scattering of Light by Small Particles. Weinheim, Germany: Wiley-VCH Verlag GmbH; 1998. ISBN 9783527618156.
[43] Patankar SV. Numerical heat transfer and fluid flow. Hemisphere Pub. Corp.; 1980. ISBN 9780891165224.
[44] Zhou HS, Honma I, Komiyama H, Haus JW. Controlled synthesis and quantum–size effect in gold-coated nanoparticles. Phys Rev B 1994;50(16):12052–6.
[45] Kreibig U, Vollmer M. Optical properties of metal clusters. Springer Series in Materials Science, 25. Berlin, Heidelberg: Springer Berlin Heidelberg; 1995. ISBN 978-3-642-08191-0.
[46] Granqvist CG, Hunderi O. Optical absorption of ultrafine metal spheres with dielectric cores. Zeitschrift for Physik B Condensed Matter and Quanta 1978;30(1):47–51.
[47] Kachan SM, Ponyavina AN. Resonance absorption spectra of composites containing metal-coated nanoparticles. J Mol Struct 2001;563–564:267–72.
[48] Khlebtsov BN, Khlebtsov NG. Biosensing potential of silica/gold nanoshells: sensitivity of plasmon resonance to the local dielectric environment. J Quant Spectrosc RadiatTransf 2007;106(1–3):154–69.
[49] Ivanova VP, Makarov IM, Schffer T, Heimburg T. Analyzing heat capacity profiles of peptide-containing membranes: cluster formation of gramicidin a. Biophys J 2003;84(4):2427–39.
[50] Oka N, Kimura K, Yagi T, Taketoshi N, Baba T, Shigesato Y. Thermophysical and electrical properties of Al-doped ZnO films. J Appl Phys 2012;111(9):093701.
[51] Robie RA, Hemingway BS, Fisher JR. Thermodynamic properties of minerals and related substances at 298.15 K and 1 bar (105 Pa) pressure and at higher temperatures. U.S. Geological Survey Bulletin; 1978.
[52] Kubaschewski O, Alcock CB, Spencer PJ. Materials thermochemistry. 6nd. Pergamon; 1993. ISBN 0080418899.
[53] Lifshitz EM, Pitaevskii LP. Physical Kinetics. 1st. Pergamon Press; 1981. ISBN 0080206417.
[54] Schöberl J. NETGEN An advancing front 2D/3D-mesh generator based on abstract rules. Comput Visualizat Sci 1997;1(1):41–52.
[55] Kourounis D, Fuchs A, Schenk O. Toward the next generation of multiperiod optimal power flow solvers. IEEE Trans Power Syst 2018;33(4):4005–14.
[56] Lee R, Aarsvold J, Chen W, Astumian R, Capelli-Schellpfeffer M, Kelley K, et al. Biophysical mechanisms of cell membrane damage in electrical shock. Semina Neurol 1995;15(04):367–74.
[57] Lombard J, Biben T, Merabia S. Threshold for vapor nanobubble generation around plasmonic nanoparticles. Phys Chem C 2017;121:15402–15.